Configurable Quadrant Photodetector: An Improved Position Sensitive Device

Roberto Esper-Chaín, Alfonso Medina Escuela, David Fariña, and José Ramón Sendra

***Abstract*— Position sensitive detectors (PSDs), used in high-end biotechnology, are based on optical sensors built over quadrant photodetectors (QPDs) or active pixel sensor (APS). These devices are intended to measure slight movements of laser spots. The QPD are, by far, the best approach in terms of resolution and noise, but requires complex and expensive *x-y* micropositioners to perform sensor alignment with the incoming laser spot. The APSs are more versatile devices that can virtually align with the spot by means of device configuration. However, due to its intrisic digital nature, the SNR and the resolutions are degraded in APS. In this paper, a new type of device called configurable QPD and its theory of operation is presented. This new device combines the analog operation of the QPD with the configurability of the APS, by means of combining photodetectors elements with analog switches in a matrix-shaped architecture. Finally, a prototype chip has been fabricated and tested and its measurements results are presented.**

***Index Terms*— Optical devices and analog circuits, optical sensors, position measurement, position sensitive devices (PSD), quadrant photodiodes (QPD), gaussian beam measurement.**

I. Introduction

NOWADAYS *position sensitive detectors* (PSDs) play an important role in high precision sensors used in many fields related with high-end biotechnology. In most of these applications, a laser beam is shot to the detector, making converge the light spot in the center of detection area of the sensor. This spot moves linked with some physical/chemical/biological parameter variation, and so, measuring this movement, this parameter can be estimated. These movements produce changes in the irradiance detected, which is reflected in the photocurrents collected by the device. Differential measurement of these currents allow for the detection of changes of the spot. There are several applications of such sensors [1]: Laser alignment systems (used in civil engineering), atomic force microscopy [2], measurement of linear displacements, calibration of precision machinery, tracking systems for military applications and measurement systems in nanometric biosensors (microcantilevers) [3]–[9]. These detectors can be built using several types of devices such as *lateral effect photodiodes* (LEP), *quadrant photodetectors* (QPD), or array of phodiodes (*active pixel sensor*, APS).

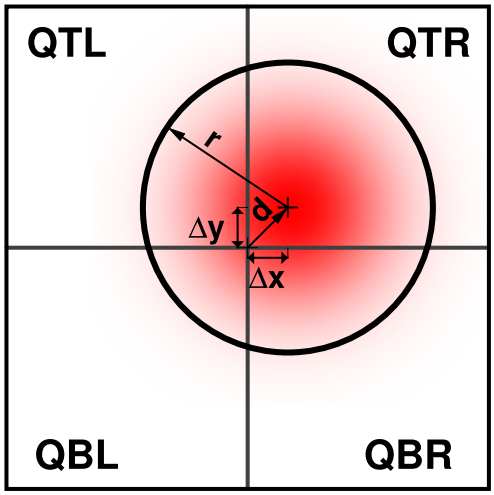

Fig. 1. Quadrant photodetector representation.

Among all the PSDs, the best approach in terms of accuracy and sensitivity is the use of QPD, represented in figure 1. This device is a fully analog sensor, that provides at its outputs the currents received by each photodetector. Their major advantage is the reduced noise floor obtained at the output of the device, allowing for improved sensitivity. Also, the use of external signal conditioning improves flexibility of the device, since gain and bandwitdh can be configured for each particular setup. As its major drawback it should be considered the needs for alignment between the device center and the spot. This requires expensive and complex x-y micropositioners that aligns the device and the spot, making sensing systems based on these devices big, expensive and complex systems. Also, only a single spot can be measured using a QPD, making unable to build multidetectors.

Alternative approaches to build a quadrant photodetector can be the use of lateral effect photodiode (LEP) or an active pixel sensor (APS). Lateral effect photodiode (LEP) provides wider detection ranges although reduced sensitivity [10]–[13]. On the other hand, APS are matrices of pixels in the same way as a CMOS Image Sensors (CIS) [14], [15]. The advantage of

Manuscript received July 20, 2015; revised August 23, 2015; accepted August 25, 2015. Date of publication September 1, 2015; date of current version December 10, 2015. This work was supported by the Consejo Superior de Investigaciones Científicas under Grant TEC2012-34280. The associate editor coordinating the review of this paper and approving it for publication was Prof. Kazuaki Sawada.

R. Esper-Chaín, A. Medina Escuela, and J. R. Sendra are with the Institute for Applied Microelectronics (IUMA), University of Las Palmas de Gran Canaria, Las Palmas 35001, Spain (e-mail: esper@iuma.ulpgc.es; aescuela@iuma.ulpgc.es; jrsendra@iuma.ulpgc.es).

D. Fariña is with the Biomedical Research Networking Center in Bioengineering, Biomaterials and Nanomedicine (CIBER-BBN), Madrid, Spain, and also with the Nanobiosensors and Bioanalytical Applications Group, Institut Catala de Nanociencia i Nanotecnologia (ICN2), CSIC, Barcelona 08193, Spain (e-mail: dfarinas@cin2.es).

Color versions of one or more of the figures in this paper are available online at http://ieeexplore.ieee.org.

Digital Object Identifier 10.1109/JSEN.2015.2475597

this approach is that the center of the spot can be digitally detected and thus, the device can be electronically aligned. Basically, once the center of the spot is located, a set of four groups of pixels can be associated together conforming four areas around the spot center, is a quadrant photodetector style [16]. Another advantage of this approach is that dark areas can be discarded, avoiding their contribution to the noise floor of the device [17]. Also, this approach is capable to manage several spots in a single device. The major drawback of the APS is related to its digital nature and the needs for high speed clocks, which are relevant noise sources. All the operations are digitally performed, increasing the noise floor of the device. So APS allows for cheaper and less complex setups, but with reduced sensitivity.

In this article, the development on a new type of device is presented. It allows to select active areas in a digital manner, but operates as an analog quadrant photodetector, collecting analog currents of each sensor element to their associated sensor. Also, the current of elements with too low irradiance received can be discarded, since they only contribute to increase the noise floor. The design, named *Configurable Quadrant Photodetector (CQPD)* is an alternative solution to PSD sensors, combining the advantages of devices based analog QPD in terms of accuracy, and the flexibility of active pixel sensor (APS), avoiding the needs of x-y micropositioners. A proof concept have been designed, fabricated and tested, and a patent application have been filed for this concept [18].

II. Quadrant Photodetectors

A. Principles & Operation

A *Quadrant Photodetector* (QPD) is a device composed by four elements arranged in quadrant, used mainly for tracking incident laser beams [19]. When a laser spot illuminates the QPD, each sensor element will provide an analog signal proportional to the optical power received. A representation of the principle of a QPD is symbolically shown in figure 1. In this figure there are four areas respresenting each sensor element, named *QTL (top-left)*, *QTR (top-right)*, *QBL (bottom-left)* and *QBR (bottom-right)*, and an incident laser spot represented by a circle of radius r. The spot center is displaced a certain distance $\{\Delta x, \Delta y\}$ from the sensor center [20]. In this situation each sensor element gets a part of the total energy received by the device. The power density over the each point on sensor will depend on the laser spot profile. Assuming that the incident beams forms an ideal circular gaussian spot, it can be equated as:

$$p(d) = \frac{2P_I}{\pi r} e^{-2d^2/r^2} \tag{1}$$

where $p(d)$ is the density of incident power at distance d from the spot center, P_I is total incident power, and r is the spot radius, defined as the distance from the spot center, where the power density downfalls by a factor of $1/e^2$. With this configuration, the power received by each sensor element can be computed as:

$$P_S = \frac{2P_I}{\pi r} \int_S e^{-2d^2/r^2} dS \tag{2}$$

Considering that in figure 1 the distance d follows $d^2 = \Delta x^2 + \Delta y^2$, the solution for the top-right element (QTR) can be obtained from:

$$P_{TR} = \frac{2P_I}{\pi r} \int_{x=-\Delta x}^{\infty} \int_{y=-\Delta y}^{\infty} e^{-2\frac{x^2+y^2}{r^2}} dx \cdot dy \tag{3}$$

which gives:

$$P_{TR} = \frac{P_I}{4} \left[1 + erf\left(\Delta x \frac{\sqrt{2}}{r}\right)\right] \left[1 + erf\left(\Delta y \frac{\sqrt{2}}{r}\right)\right] \tag{4}$$

And thus:

$$\begin{cases} P_{TL} = \frac{P_I}{4} \left[1 - erf\left(\Delta x \frac{\sqrt{2}}{r}\right)\right] \left[1 + erf\left(\Delta y \frac{\sqrt{2}}{r}\right)\right] \\ P_{BR} = \frac{P_I}{4} \left[1 + erf\left(\Delta x \frac{\sqrt{2}}{r}\right)\right] \left[1 - erf\left(\Delta y \frac{\sqrt{2}}{r}\right)\right] \\ P_{BL} = \frac{P_I}{4} \left[1 - erf\left(\Delta x \frac{\sqrt{2}}{r}\right)\right] \left[1 - erf\left(\Delta y \frac{\sqrt{2}}{r}\right)\right] \end{cases} \tag{5}$$

When the spot center is perfectly aligned with the QPD center, each quadrant photodetector receives $1/4$ of the total incident power over the sensor. However, if the spot moves, the power received by each element varies, and the displacement can be deducted from:

$$\begin{cases} \Delta x \equiv (P_{TR} + P_{BR}) - (P_{TL} + P_{BL}) = P_R - P_L \\ \Delta y \equiv (P_{TR} + P_{TL}) - (P_{BR} + P_{BL}) = P_T - P_B \end{cases} \tag{6}$$

For instance, in order to obtain the value of Δx, we should compute the difference of the power received between right (P_R) and left halves (P_L) of the device:

$$\begin{cases} P_R = \frac{P_I}{2} \left[1 + erf\left(\Delta x \frac{\sqrt{2}}{r}\right)\right] \\ P_L = \frac{P_I}{2} \left[1 - erf\left(\Delta x \frac{\sqrt{2}}{r}\right)\right] \end{cases} \tag{7}$$

So we can compute the power difference between halves as:

$$\begin{cases} \Delta P_H = (P_R) - (P_L) = P_I \cdot erf\left(\Delta x \frac{\sqrt{2}}{r}\right) \\ \Delta P_V = (P_T) - (P_B) = P_I \cdot erf\left(\Delta y \frac{\sqrt{2}}{r}\right) \end{cases} \tag{8}$$

Where, ΔP_H is the horizontal power deviation, and ΔP_V is the vertical one. Finally, the relationship between the spot displacement and the power variation received by each pair of halves follows:

$$\begin{cases} \Delta x = \frac{r}{\sqrt{2}} erf^{-1}\left(\frac{\Delta P_H}{P_I}\right) \\ \Delta y = \frac{r}{\sqrt{2}} erf^{-1}\left(\frac{\Delta P_V}{P_I}\right) \end{cases} \tag{9}$$

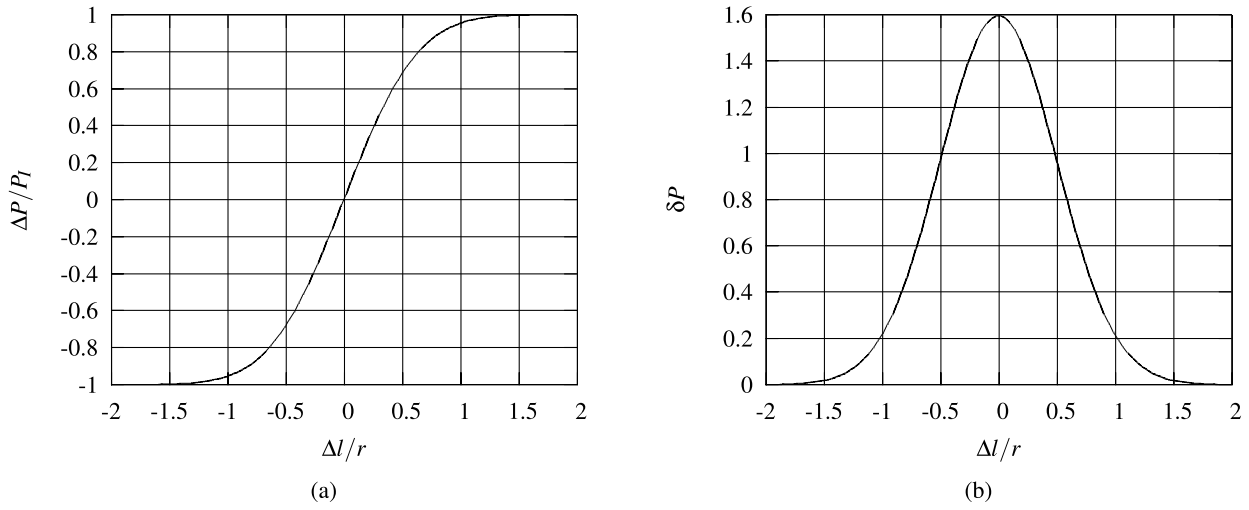

Fig. 2. QPD operation: (a) relationship between power variation between halves and spot displacement and (b) sensitivity versus spot displacementacross the device.

B. Discussion

In figure 2(a) it is shown the theorical normalized power difference ($\Delta P/P_I$) between halves (according to equation 8) related to the center of the spot displacement. In figure 2(b) the displacement sensitivity is presented, estimated as the derivation of the power variation (δP) shown in figure 2(a). It should be noticed that displacements beyond $1.5 \times r$ are almost undetectable. Moreover, the maximum sensitivity is obtained around 0. Also, good sensitivity can obtained for displacements within ranges $[-r/2, r/2]$. Outside that range, sensitivity falls quickly to zero. Controlling the spot radius may control the measurement range but also the measurement resolution. The bigger the spot, the wider the measurement range, but the smaller the sensitivity. Choosing the spot size (when possible), should be done as a trade-off between measurement range and measurement sensitivity. For instance, when very good sensitivity is required, well focused spots, with reduced radio r, should be used, but then, only small displacement ranges can be measured.

In order to perform a measurement with a QPD sensor, a mechanical calibration process is required. In this process, the centers of the laser spot and the QPD must be aligned. In most of the applications this process should be done by means of x-y micropositioners, increasing cost and complexity of the measurement system. This aligment process is critical, and the resolution of the x-y micropositioners should be increased when reduced spot sizes are used, increasing the overall system cost.

III. Configurable Quadrant Photodetector Architecture

A. Introduction

In order to avoid the mechanical calibration, a device that emulates the movement of the center of the QPD by electronic means is proposed. Also, this device will allow for extended movement detection, spot size calibration, as well as multispot detection, as it will be discussed further in detail.

B. Proposed Architecture

The proposed sensor design combines the sensitivity and accuracy of QPDs with the flexibility and reduced cost of implementations based on image sensors. Figure 3(a) shows the structure of the proposed device, where its core is composed by a matrix of photodetectors or *sensor elements*, a set of interconnection channels per row, and a set of analog switches that connect the sensor elements to the proper channels. On the device periphery, a set of configuration flip-flops, connected in daisy chain allows to configure the device. This digital interface loads serially a sensor configuration to configure the analog switches. Once configured, the digital logic is stopped, so the digital noise is muted. The remaining logic operates statically, so no switching noise interferes with the measurement. From this point of view, the device behaves as a pure analog sensor. Four big groups of photodiodes elements are short-circuited to each output in a quadrant photodetector style. Each of the four outputs give the addition of the photocurrents of sensor elements connected to them, so no quantification error is injected. No A-to-D converter nor conditioning electronic is included. The key point of the proposed architecture, is that the digital configuration allows to match the sensing area to the center and size of the spot, and to reuse conditioning chains for standard QPS, but without the needs for any micromechanical adjustment.

As can be see in detail in figure 3(a), most of the area of the device is dedicated to the sensor elements. These elements are photodiodes, occupying most of the sensor element surface. Each row of sensor elements has associated a *horizontal channel pair* named *connection to the right* (`r_n`) and *connection to the left* (`l_n`). Each sensor element has a pair of switches to short-circuit the photodiodes to one of each channel (*to the right* or *to the left*). If none of the switches are selected a third switch ties the photodiode to ground, allowing to discard elements where no significant signal power is obtained, matching the sensing area to places where significative power is received.

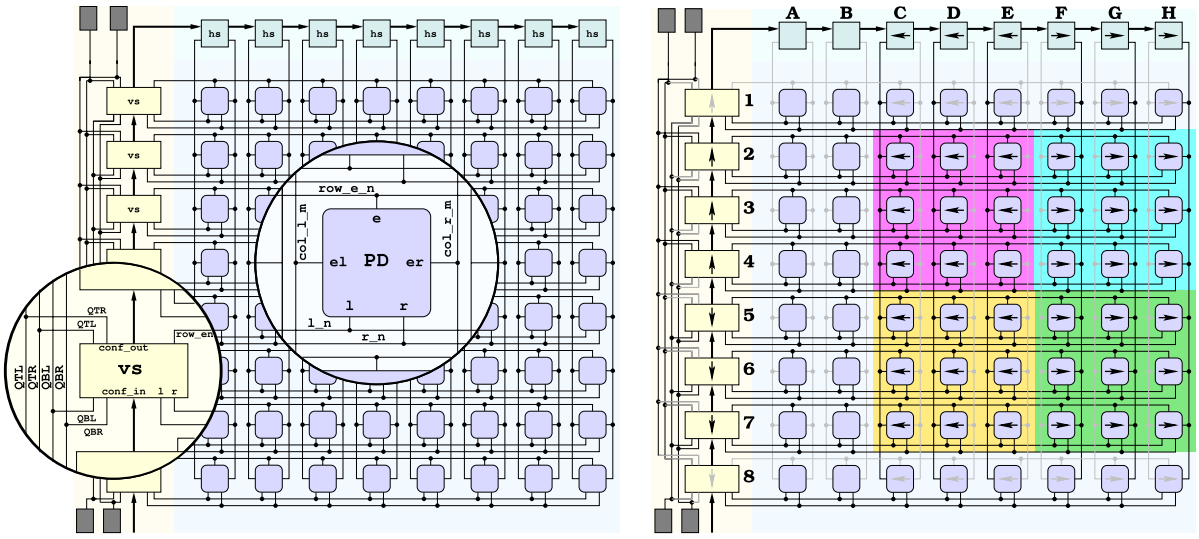

(a) (b)

Fig. 3. (a) Simplified diagram of the Configurable Quadrant Photodetector and (b) sample configuration.

Each *horizontal channel pair* is connected to a vertical switching unit. Each unit can connect to a pair of outputs at *top* (QTR & QTL) or at *bottom* (QBR & QBL) their associated *horizontal channel pair*. Also, some specific channels can be discarded. In the proposed device, switches on the sensor elements can be configured per columns, so each sensors elements column can send its current *to the right* or *to the left* through dedicated channels per row. Each *vertical switching* has its own configuration.

In short, in the proposed device has four outputs as a classical QPD, and can be configured:

- Each column can be connected *to the right*, *to the left* or discarded.
- Each row can be connected *top*, *bottom* or discarded.

Figure 3(b) shows a sample configuration. First of all, it should be noted the column configuration at the top of the schematic:

- The two leftmost columns (A & B) are configured to discard the signal.
- The following three columns (C, D & E) are configured to send their current *to the left*.
- The three rightmost columns (F, G & H) are configure to send their current *to the right*.

Each set of channels reach to a single vertical switching unit. Each vertical switching unit can take on of the following options:

- Discard the incoming current (such as shown in rows 1&8).
- Connect to *top* (such as shown in rows 2, 3 & 4). In this case:
  - *Right channel* is sent to the *QTR* output.
  - *Left channel* is sent to the *QTL* output.
- Connect to *bottom* (such as shown in rows 2, 3 & 4). In this case:
  - *Right channel* is sent to the *QBR* output.
  - *Left channel* is sent to the *QBL* output.

With sample configuration shown the effect obtained is:

1) The *QTR* output will be physically connected to the {F2:H4} sensor elements.
2) The *QTL* output will be physically connected to the {C2:E4} sensor elements.
3) The *QBR* output will be physically connected to the {F5:H7} sensor elements.
4) The *QBL* output will be physically connected to the {C5:E7} sensor elements.
5) The current sensed by elements in columns A & B will be discarded by the sensors themselves.
6) The current sensed by elements {C1:H1} & {C8:H8} will be discarded by their vertical switching units.

It should be noted that all sensor elements within a quadrant are short-circuited to the associated output. The configuration is hold by static flip-flops, so once programmed, remains static while the measurement is in progress.

C. Mathematical Model

In order to model the operation of the proposed device, it should be computed the power received by each sensor element. To get this, first consider the symbolic model shown in figure 4(a). Solving equation 3, to compute P_A, which is the the part of the total power P_T incident over the area A:

$$P_A = \frac{P_T}{2}\left[1 + erf\left(x_o\frac{\sqrt{2}}{r}\right)\right] \tag{10}$$

and therefore, the power P_S incident over the segment S, (x_o, y_o) is the corner of the sensor element, and w & h are the width and height of the sensor elements.

$$P_S = \frac{P_T}{2}\left\{erf\left[(x_o + w)\frac{\sqrt{2}}{r}\right] - erf\left(x_o\frac{\sqrt{2}}{r}\right)\right\} \tag{11}$$

Extending this solution to the general model, shown in figure 4(b), the power received by each sensor element can

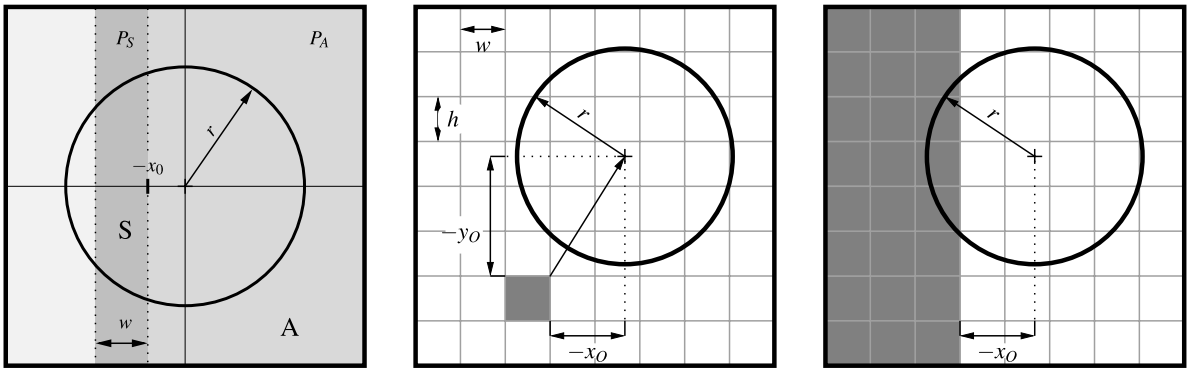

(a) (b) (c)

Fig. 4. Configurable Quadrant Photodetector modeling: (a) estimation of the power receiver by segments, (b) estimation of the power received by each sensor element and (c) configuration for horizontal displacement detection.

be computed as:

$$\begin{cases} P_E = \dfrac{P_T}{4}\left\{erf\left[(x_o+w)\dfrac{\sqrt{2}}{r}\right] - erf\left(x_o\dfrac{\sqrt{2}}{r}\right)\right\} \\ \qquad \times\left\{erf\left[(y_o+h)\dfrac{\sqrt{2}}{r}\right] - erf\left(y_o\dfrac{\sqrt{2}}{r}\right)\right\}. \end{cases} \tag{12}$$

D. Proposed Device Characteristics

The configurability of the device provides with value added advantages. In this section the advantages of the proposed device are discussed.

1) Calibration: With the proposed device it is possible to align the center of the spot with the center of the device, avoiding the use of micromechanical facilities, which greatly simplifies the design and setup of laser beams position measurements, which was the primary goal for the proposed design.

2) Active Area Limitation: Another advantage of the proposed device over the classical QPD, is the capability to discard sensor elements where no significant signal is received, and thus, limiting the active area of the sensor to places where signal to noise ratio is significative. This will reduce noise and dark current contributions to the measurement.

3) Advanced Configurations: The configurability of the device allows for special configurations for movement detection. For instance, in figure 4(c) the device is configured for horizontal spot displacement detection. With this configuration only two analog channels are required, implementing the estimation presented in equation 8, easing the design of the external conditioning chain & setup. In the figure 4(c), a sample configuration is shown where, 3 elements are selected to the left, and the remaining 5 to the right. The adjustment can be done based on the spot position, depending on the measurement setup requirement.

In order to perform a vertical displacement detection, an equivalent configuration can be found. Performing mutiplexed horizontal & vertical measurements, it is possible to operate with only two channels but still getting full $(\Delta x, \Delta y)$ detection.

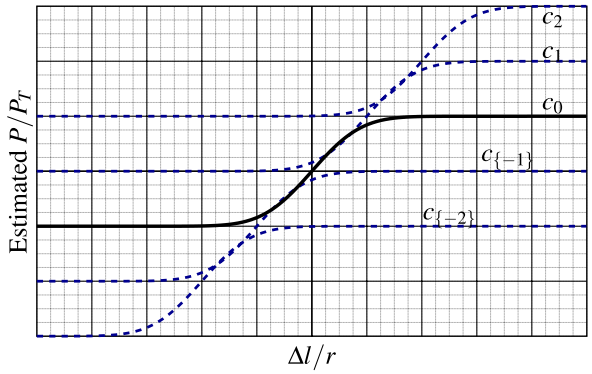

Fig. 5. Extended range detection.

4) Extended Range Detection: It is possible to perform a electronic tracking of the center of the spot. As discussed earlier on section II-B, on a classical QPD there was a trade-off between detection range and resolution. The smaller the spot radius (r), the better the detection resolution, but the worse the range (which it's limited beyond $[-3r/2, 3r/2]$). However, the proposed device has a *moveable* center, so it is possible to increase the resolution. In figure 5, a representation of the extended range is shown. Curve c_0 shows the simulation of a calibrated classical QPD. Curves c_1, c_2, $c_{\{-1\}}$ & $c_{\{-2\}}$, show the estimated simulation for moved centers. These curves are vertically drifted to illustrate center displacement and thus the extended measurement range. The number of curves obtained depend on the number of rows an columns available on the device.

5) Spot Size Estimation: With this device is possible to estimate the spot size, which can lead to more accurate measurements, and can help to calibrate the optical front-end. The calibration of the spot size should be performed in two phases, obtaining estimated measurement for r_x and r_y, since spots are commonly not circular but elliptic.

There are several works about spot size estimation using classical QPDs and some mechanical movements of the device [21]–[24]. However the configurability of the CQPD with extra flexibility to estimate the the horizontal size of the spot (r_x). Several algorithms can be found. In the pesented

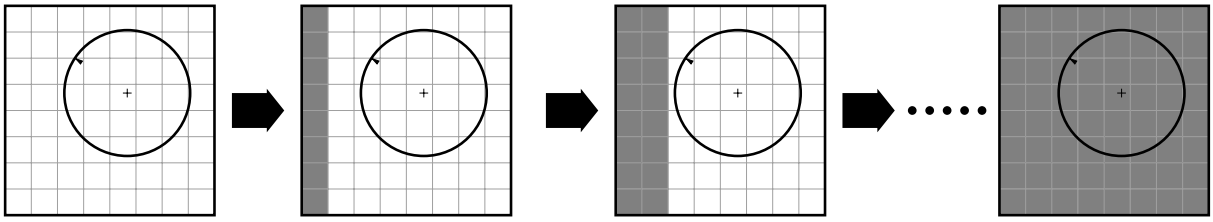

Fig. 6. Horizontal scanning for spot size estimation.

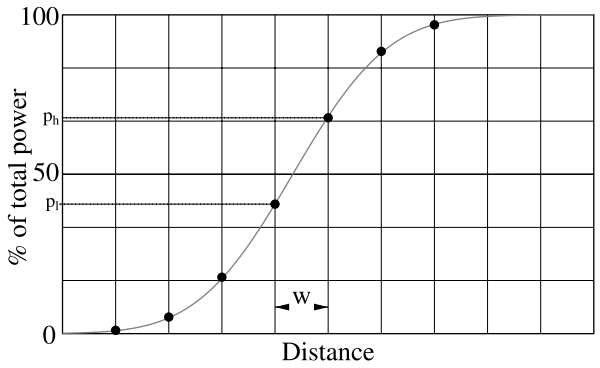

Fig. 7. Measurements for spot size estimation.

work a sample algorithm was used, based on a set of horizontal measurements or *scanning* of the spot, based on the configuration proposed in figure 4(c). With this algorithm used is not required to know where the center of spot is located, however the spot should be entirely located within the device.

It starts measuring in a single channel (for instance *top-left*) with nothing connected to it, (to calibrate the offset level), then with the left-most column connected to it, then with the two left-most, and so forth, until the last measurement is perfomed with all the sensor elements short-circuited to the *top-left* output. Figure 6 shows symbolically this scanning process. At the end of the process, a set of values is obtained, that should match equation 8, as shown in figure 7, where measured points are drawn in black, and the underlying error function is drawn in grey. Several techniques can be used to estimate the value of the spot radius. For instance, the two closest point to the 50%, can be taken, since these are the points where maximum resolution is offered by the error function (p_l and p_h in the graphic). From equation 8 it can be obtained:

$$\begin{cases} v_l = erf^{-1}\left(\dfrac{p_l}{P_T}\right) \\ v_h = erf^{-1}\left(\dfrac{p_h}{P_T}\right) \end{cases} \tag{13}$$

And combining this equation with equation 9 gives:

$$v_h - v_l = \frac{\sqrt{2}}{r_x}(x_h - x_l) \tag{14}$$

But $x_h - x_l = w$, where w is the horizontal size of the sensor element, so it can concluded that:

$$r_x = \frac{\sqrt{2}\cdot w}{v_h - v_l} \tag{15}$$

In the same way, a vertical scanning of the spot will estimate the vertical spot radius r_y, which in real systems, as said before, not necessarily has to be matched to the horizontal one.

6) Multispot Emulation: With this device it is possible to perform the detection of several spots. As soon as these spots do not interfere each other, it is possible to select only specific areas for each spot, discarding areas with no significant power or where undesired spots are received. It should be noted that most of the biological signals evolves at low rates, (seconds or slower). Switching configurations among spot centers will allow to emulate multispot detection in a multiplexed manner.

Moreover, it is possible to extend the architecture presented to perform a true multispot detector, multiplying the number of horizontal & vertical chanels, as well as redesigning the switching & configuration units.

E. Implementation

A prototype chip has been designed. In figure 8 detailed schematics of this prototype are shown. In figure 8(a) a detailed schematic of the transmission gates used as analog switches is shown. The MOS transistors were sized for the expected current in the system. In figure 8(b) a schematic of each sensor element is shown. Most of the area of the element is occupied by a photodiode in common anode configuration. Some logic selects whether the cathode of the photodiode is short-circuited to the *left* or the *right* channel, or discarded. In figures 8 (c), (d) & (e), the periphery configuration logic are shown. All the preload flip-flop are connected in daisy chain, allowing loading configurations by means of serial transmission. When the configuration is completeley loaded, a `load` signal transfer the values to the load flip-flops, taking effect this new configuration at once. Figure 9 shows a photo of the fabricated chip. This prototype is composed by a matrix of 400 elements organized in 20×20 elements. It have been fabricated using Austria Microsystems *C35OPTO* process ($0.35\mu m$), with 14720 transistors, 160 flip-flops and 400 photosensors. It was packaged in a DIP28 with an open window to allow the device to be exposed to the light. The configuration is loaded using a standard LVCMOS 3.3V SPI port, available in most of commercial microcontrollers. The area of the chip is $5mm^2$. Each sensor element has an area of $75.8\mu m \times 75.8\mu m$, with a fill factor of the sensing area of about the 78% of the element ($\approx 4500\mu m^2$). According to Austria Microsystems, the device is expected to deliver about $400mA/W$ for $650nm$ wavelength.

IV. Experimental Results

A. Experimental Setup

A experimental test plan for this prototype has been run. For this test plan, a custom optical setup has been designed.

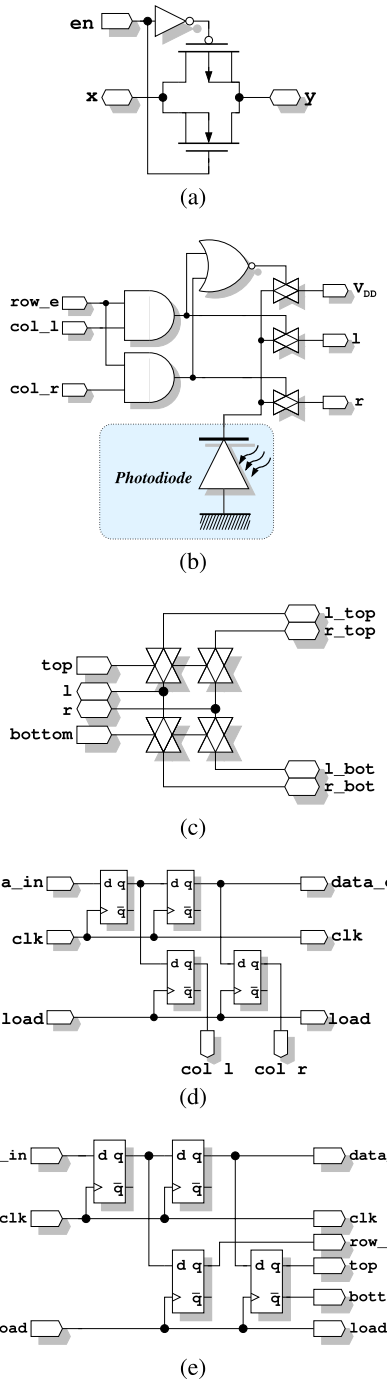

Fig. 8. Detailed implementation of the CQPD prototype: (a) Analog switch, (b) sensor element, (c) vertical switching, (d) column control and (e) row control.

All components of the optical setup (light sources, beam splitter, beam expander and CQPD DUT) are mounted on top of the optical posts and then, inserted into the post holder on an optical breadboard, to facilitate alignment of all the devices in the desired configuration. Figure 10 show the assembled configuration. A laser beam is confined in a beam expander (Thorlab BE10M-B) whose exit path go through an optical splitter, located in a glue-in 4-port prism cage cube mount. This splitter will allow projecting the incident spot on the surface of a perpendicular CQPD DUT, in order to find the actual

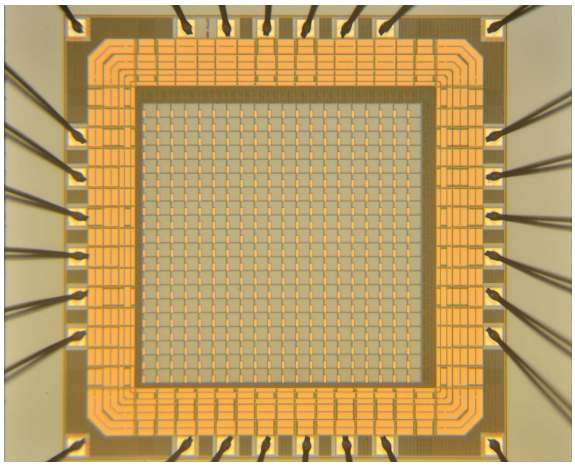

Fig. 9. CQPD prototype die photo.

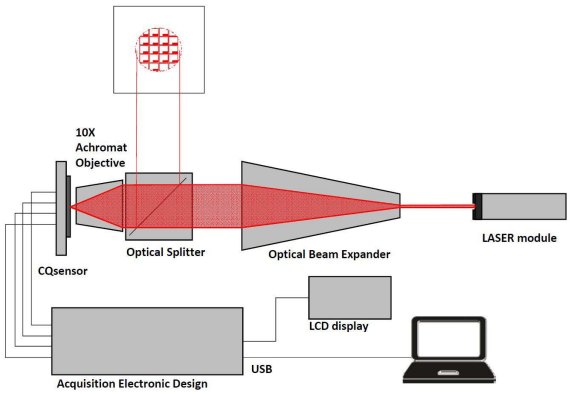

Fig. 10. Experimental setup.

sensor surface covering by spot plane. On leaving the splitter, the spot is focused in the region of interest (Olympus 10X objective plan achromat). The optical power delivered measured with a optical power meter (Thorlab S20MM) at the surface of CQPD was $355\mu W@635nm$.

The CQPD signals are connected to an custom electronics acquisition system designed for this setup, through U.FL electrical connectors (U.FL-R-SMT(10) from Hirose) and special wires that carry the photocurrents. A flat cable controls the programming of CQPD. The electronics acquisition system is composed by four chains of transimpedance amplifers, signal conditioning, low pass filters (Sallen-Key, fourth order) and 12-bit ADC controlled by an ARM Cortex-M3 processor with USB capability [25]. The acquisition system transfers measurement data to a local computer by means of USB connection. The total current measured at the output of the CQPD was $112\mu A$, which gives an estimated responsivity of $\approx 315mA/W$. Taking into account that the each photodiode occupies the 78% of each sensor element, results in an estimated responsivity of $\approx 404mA/W$ for the technology, which is coherent with the specification from Austria Microsystems for $635nm$.

Since large sensor elements were used, no *dead-pixels* were expected. These *dead-pixels* can be detected performing a scan using 1×1 quadrant configuration, and a uniform

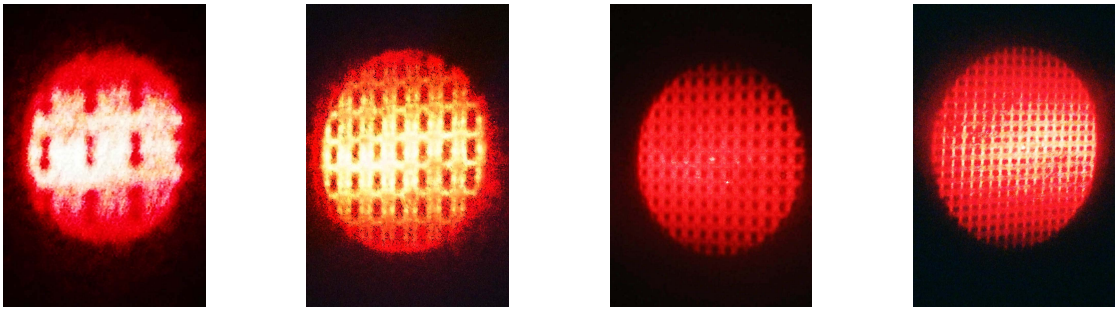

≈ 3 elements wide ≈ 7 elements wide ≈ 13 elements wide ≈ 18 elements wide

Fig. 11. Spots used for spot size estimation setup.

TABLE I
SPOT SIZE MEASUREMENT RESULTS

Wide	Measured size $\mu m \times \mu m$)	h/w	figure
3	$(96.9 \pm 0.7) \times (191.6 \pm 0.9)$	1.98	32.3
7	$(187.3 \pm 1.4) \times (394.7 \pm 4.1)$	2.11	26.8
13	$(330.1 \pm 3.1) \times (687.9 \pm 13.4)$	2.08	25.4
18	$(473.1 \pm 4.4) \times (991.7 \pm 19.6)$	2.10	26.3

light source. No dead-pixel were found on any of the devices tested. However, when using small spots sizes, dead-pixel aligned with spot centers can produce critical errors on the measurements. So devices with dead-pixels should be discarded.

B. Spot Size Estimation

As discussed earlier, in section III-D5, it is possible to detect the size of the spot, scanning the spot in the x & y direction. The setup to carry out this measurement requires to perform vertical & horizontal scannings to determine the size of the spot.

Based on the measurement results, the size of the spot can be computed using equations 13-15. A this point, it should be noticed that in our setup, we haven't capability to determine precisely the spot size to verify the accuracy of our estimations. We only have an projected image of the spot, as shown in figure 11, where we can count how many sensor elements are included within the spot, but we cannot determine accurately the limits of the spot according to the gaussian beam definition. However, we should find a correlation between the measured size and the number of sensor elements visible in the projection. Also, a constant ratio between x & y sizes should be obtained.

To run the test, we configure the spot to make visible 3, 7, 13 & 18 sensor elements in the projection in the x-direction, and positioned the spot at the center of the device. We run the test and perfom 10 measurements at each configuration.

Results are shown in table I. In this table, the column h/w shows the measured ratio between the height & width of the spot, which is known to be constant. Results show a stable value within 2.5% of standard deviation. Moreover, the column *figure* shows the ratio between the actual measured width of the spot (in microns) and visible width of the spot (in elements). This figure should give a constant value. Results are again consistent with the model. Also, it should be noticed that the result obtained for 3 sensor elements wide, is slightly apart from the rest, but also it should be considered that relatives unaccuracies in the manual spot size adjustment process is more relevant when smaller spot sizes are used.

Also, according to the theory developed on section III-D, with this device it is possible to perform an analog scanning of the spot to match how gaussian this spot is. Based on the spot size measurement presented in previous section, a comparison between the ideal gaussian spot and the actual measured spot can be performed. The results are shown in figure 12. These results are consistent with the expected operation.

C. Position Detection

The main application for *classical quadrant photodetectors* is the detection of the position of a single laser spot. As discussed earlier in section II-B and in shown in figure 2, the detection range on traditional QPDs depends on the spot size, so the smaller the spot, the smaller the detection range. Good accurary is expected when the spot center is not further than $\pm r/2$ from the device center.

In this setup, two measurements have been performed, *x-displacement* and *y-displacement*. On the *x-displacement* test, the spot is centered in the y axis, and moved $\approx 1250\mu m$ in 25 steps from on left to right ($\Delta x \approx 50\mu$ per step). The device is configured as a simple classical QPD, with four fixed quadrants of 10×10 sensor elements. On the *y-displacement* test, the spot is centered in the x axis and moved from top to bottom in the y direction.

A total of 500 measurements have been performed, 10 per position (25 steps on the x-displacement test and so 25 on the y-displacement test). The spot used had a estimated size of $97.5\mu m \times 188.0\mu m$. Results shows the positions estimated by the device are shown in figure 13. As shown in the figure, there are more usable detected points on the y direction since the spot size is approximately two times larger than on the x direction. The results are coherent with the predicted operation of the device.

D. Extended Position Detection

As discussed in section III-D4, and improvement of the proposed device over the classical QPDs is the ability to extend the range of detection. To demonstrate this capability,

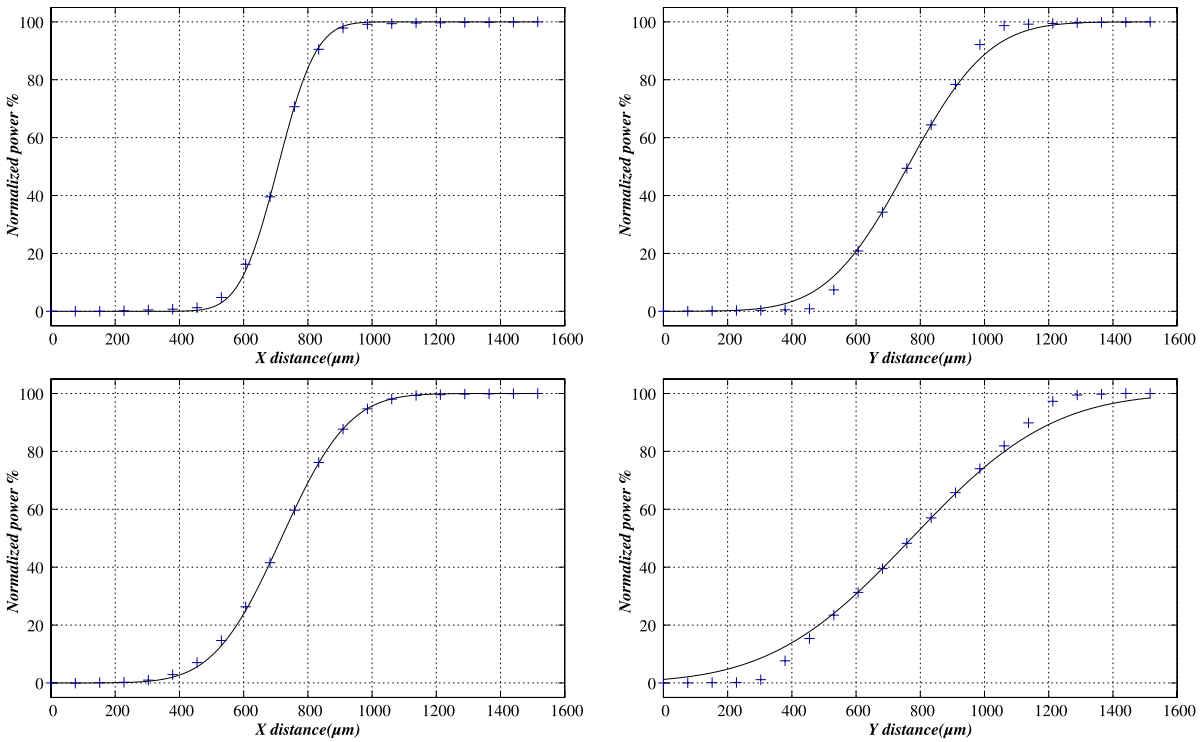

Fig. 12. Spot matching test results: Comparison between ideal signal (line) and measured values (marks) for (a) horizontal and (b) vertical scan for 7 (top) and 13 (bottom) elements wide spot.

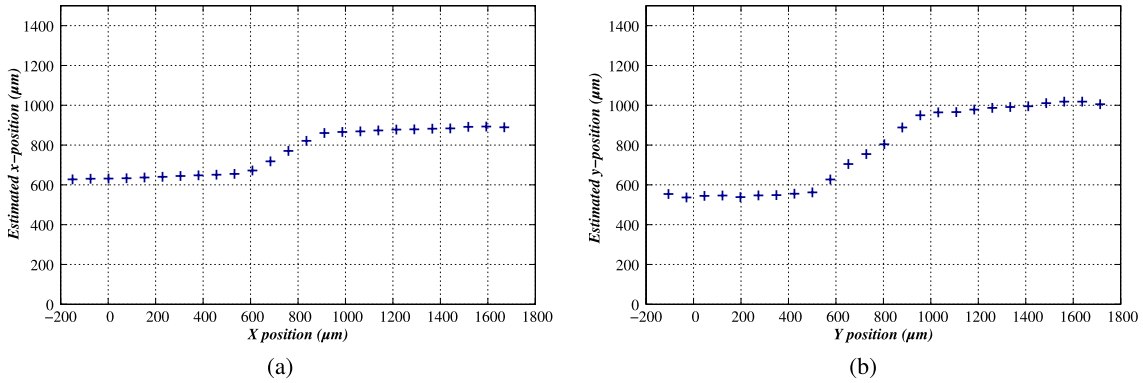

Fig. 13. Positions detected on a fixed QPD configuration: (a) x-displacement and (b) y-displacement.

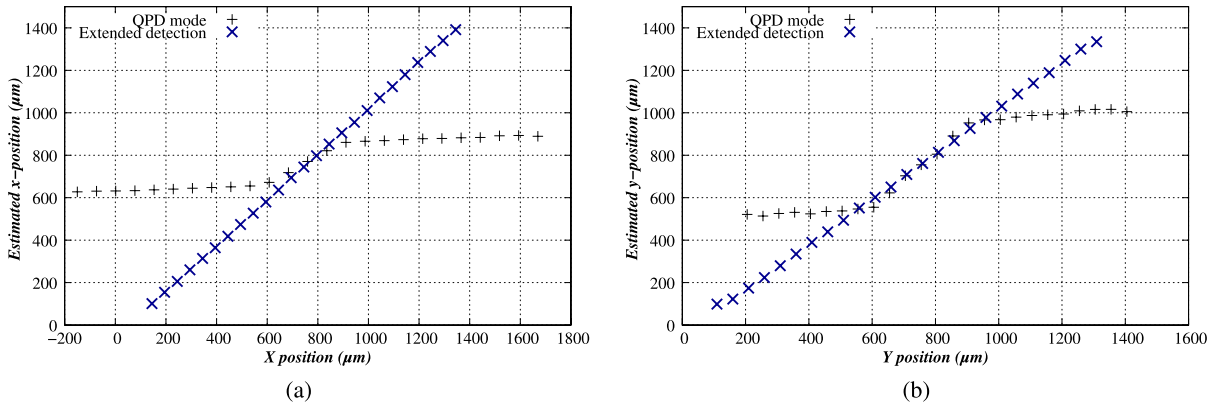

Fig. 14. Positions detected on a extended CQPD configuration compared with fixed QPD configuration: (a) x-displacement and (b) y-displacement.

the same test used the precedent section has been repeated, but performing the spot scanning shown in figure 6. A set of 21 configurations are used per measurement, ranging from device off to full device short-circuited to one single channel. The estimated positions versus the actual positions are shown in figure 14. Also, in this figure, a comparison with the

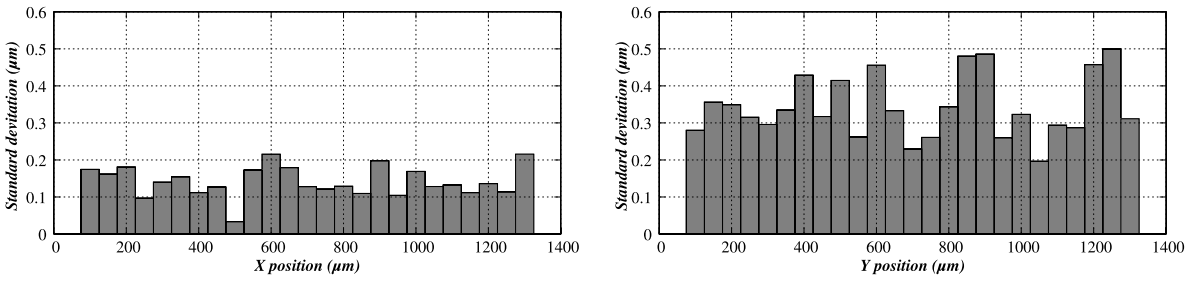

(a) (b)

Fig. 15. Extended range measurement dispersions (a) X-axis and (b) Y-axis.

classical QPD configuration is shown, where the adventages of the advanced configuration over the classical approach is obvious. Also, the sensisitivity could be improved reducing the spot size, without reducing the detection range.

On each point, a set of repeated measurements was performed in order to estimate the resolution obtained. The dispersion of these measurements was very low (as expected), with values always below $1\mu m$ in the y direction & always below $300nm$ in the x direction, a representation of this dispersion is shown in figure 15. It can be observed that the resolution is much better in the x direction, and that is related to the fact that the spot radius is smaller in that direction. This is consistent with the discussion in section II-B and what was shown in figure 2(b).

Results show a lineal, and very precise operation, and a range extended consistent with the theory discussed in this article.

V. Conclusion

In this article, the use of a *Configurable Quadrant Photodetector* (CQPD) is proposed, in order to improve the characteristics of *position sensitive devices* (PSDs), avoiding the needs for spot aligment using complex x-y micropositioners, getting rid of the usual trade-off between sensibility and dynamic range. Their theory of operation is presented, showing the benefits of the proposed device architecture, and some extra value-added features such as extended range detection, spot size estimation & matching, as well as multispot operation.

A prototype has been designed and fabricated, which was composed by a matrix of 400 elements organized in 20×20 elements using Austria Microsystems *C35OPTO*. Its sensivite area was $\approx 1.5mm \times 1.5mm$, enough to verify the concept operation. Experimental tests results obtained are also presented, and their correct operation has been verified.

References

[1] N. V. Lavrik, M. J. Sepaniak, and P. G. Datskos, "Cantilever transducers as a platform for chemical and biological sensors," *Rev. Sci. Instrum.*, vol. 75, no. 7, pp. 2229–2253, 2004.

[2] H.-J. Butt, "A sensitive method to measure changes in the surface stress of solids," *J. Colloid Interf. Sci.*, vol. 180, no. 1, pp. 251–260, 1996.

[3] J. Homola, "Present and future of surface plasmon resonance biosensors," *Anal. Bioanal. Chem.*, vol. 377, no. 3, pp. 528–539, 2003.

[4] A. Escuela, J. Sendra, E. Mauriz, A. Calle, and L. Lechuga, "Portable prototypes of surface plasmon resonance biosensors applications in the environmental control," in *Proc. 7th Conf. Opt., Chem. Sensors Biosensors*, 2004.

[5] H. Q. Zhang, S. Boussaad, and N. J. Tao, "High-performance differential surface plasmon resonance sensor using quadrant cell photodetector," *Rev. Sci. Instrum.*, vol. 74, no. 1, pp. 150–153, 2003.

[6] H.-F. Ji, K. M. Hansen, Z. Hu, and T. Thundat, "Detection of pH variation using modified microcantilever sensors," *Sens. Actuators B, Chem.*, vol. 72, no. 3, pp. 233–238, 2001.

[7] G. C. M. Meijer, J. van Drecht, P. C. de Jong, and H. Neuteboom, "New concepts for smart signal processors and their application to PSD displacement transducers," *Sens. Actuators A, Phys.*, vol. 35, no. 1, pp. 23–30, 1992.

[8] C. Carbonell, I. Imaz, and D. Maspoch, "Single-crystal metal–organic framework arrays," *J. Amer. Chem. Soc.*, vol. 133, no. 7, pp. 2144–2147, 2011.

[9] A. B. González-Guerrero, M. Alvarez, A. G. Castaño, C. Domínguez, and L. M. Lechuga, "A comparative study of in-flow and micropatterning biofunctionalization protocols for nanophotonic silicon-based biosensors," *J. Colloid Interf. Sci.*, vol. 393, pp. 402–410, Mar. 2013.

[10] A. Mäkynen, J. T. Kostamovaara, and R. A. Myllylä, "Displacement sensing resolution of position-sensitive detectors in atmospheric turbulence using retroreflected beam," *IEEE Trans. Instrum. Meas.*, vol. 46, no. 5, pp. 1133–1136, Oct. 1997.

[11] W. Wang and I. J. Busch-Vishniac, "The linearity and sensitivity of lateral effect position sensitive devices-an improved geometry," *IEEE Trans. Electron Devices*, vol. 36, no. 11, pp. 2475–2480, Nov. 1989.

[12] J. Henry and J. Livingstone, "A comparison of layered metal-semiconductor optical position sensitive detectors," *IEEE Sensors J.*, vol. 2, no. 4, pp. 372–376, Aug. 2002.

[13] H. A. Andersson, K. Bertilsson, G. Thungstrom, and H.-E. Nilsson, "Processing and characterization of a MOS-type tetra lateral position sensitive detector with indium tin oxide gate contact," *IEEE Sensors J.*, vol. 8, no. 10, pp. 1704–1709, Oct. 2008.

[14] A. Makynen and J. Kostamovaara, "An application specific PSD implemented using standard CMOS technology," in *Proc. IEEE Int. Conf. Electron., Circuits Syst.*, vol. 1, Sep. 1998, pp. 397–400.

[15] F. De Nisi *et al.*, "A CMOS sensor optimized for laser spot-position detection," *IEEE Sensors J.*, vol. 5, no. 6, pp. 1296–1304, Dec. 2005.

[16] D. Liping, Z. Zhou, and T. Shugang, "The characteristic analysis and optimization of quadrant detector signal," in *Proc. IEEE Int. Conf. Intell. Comput. Intell. Syst. (ICIS)*, vol. 3, Nov. 2009, pp. 190–194.

[17] A. Mäkynen and J. Kostamovaara, "Linear and sensitive CMOS position-sensitive photodetector," *Electron. Lett.*, vol. 34, no. 12, pp. 1255–1256, 1998.

[18] J. Sendra, R. Esper-Chaín, A. Medina, and J. Monagas, "Dispositivo sensor de cuadrante configurable (CQ-sensor)," Spanish Patent ES 2 400 291, Jul. 23, 2014.

[19] L. P. Salles and D. W. de Lima Monteiro, "Designing the response of an optical quad-cell as position-sensitive detector," *IEEE Sensors J.*, vol. 10, no. 2, pp. 286–293, Feb. 2010.

[20] C. B. Shen, B. G. Sun, T. J. Ma, P. Lu, S. F. Lin, and X. H. Wang, "Research of signal-processing methods in four-quadrant photodetector," in *Proc. Int. Conf. Elect. Mach. Syst. (ICEMS)*, 2008, pp. 917–919.

[21] A. K. Cherri and M. S. Alam, "Accurate measurement of small Gaussian laser beam diameters using various rulings," *Opt. Commun.*, vol. 223, nos. 4–6, pp. 255–262, 2003.

[22] H. A. Kamal and A. K. Cherri, "Measurement of a broad range of Gaussian laser beam diameters using various periodic and aperiodic rulings," *Opt. Laser Technol.*, vol. 36, no. 7, pp. 551–559, 2004.

[23] T. W. Ng, S. L. Foo, and H. Y. Tan, "Gaussian laser beam diameter measurement using a quadrant photodiode," *Rev. Sci. Instrum.*, vol. 76, no. 6, p. 065110, 2005.
[24] T. Ng, H. Tan, and S. Foo, "Small Gaussian laser beam diameter measurement using a quadrant photodiode," *Opt. Laser Technol.*, vol. 39, no. 5, pp. 1098–1100, 2007.
[25] L. Rovati, M. Bonaiuti, and P. Pavan, "Design of a high-performance optical system for angular position measurement: Optical and electronic strategies for uncertainty reduction," *IEEE Trans. Instrum. Meas.*, vol. 54, no. 5, pp. 2075–2081, Oct. 2005.

Roberto Esper-Chaín received the Telecommunication Engineering and Ph.D. degrees from the University de Las Palmas de Gran Canaria, Spain, in 1992 and 2002, respectively. He is currently an Associate Professor with the Institute for Applied Microelectronics (IUMA), University of Las Palmas de Gran Canaria. His fields of interests include development of electronics and sensor systems.

Alfonso Medina Escuela received the Telecommunication Engineering and Ph.D. degrees from the University of Las Palmas de Gran Canaria (ULPGC), in 1992 and 2011, respectively. He is currently an Associate Professor with the Institute for Applied Microelectronics (IUMA), ULPGC. His current fields of interest include development of electronics systems in biosensors signal processing.

David Fariña received the M.E. and Ph.D. degrees in telecommunications engineering from the University of Las Palmas de Gran Canaria, Spain. He is currently a Doctor-Engineer with the Biomedical Research Networking Center in Bioengineering, Biomaterials and Nanomedicine (CIBER-BBN), Madrid, Spain, and with the Nanobiosensors and Bioanalytical Applications Group at the Institut Catala de Nanociencia i Nanotecnologia (ICN2), CSIC, Barcelona, with a special interest on software and hardware development for optical biosensors and their integration in lab-on-chip platforms.

José Ramón Sendra received the Ph.D. degree from the Politechnic University of Madrid, in 1996. He is currently an Associate Professor with the Institute for Applied Microelectronics (IUMA), University of Las Palmas de Gran Canaria, Spain. He has been involved in the development of electronic instrumentation for optical biosensors. He is Co-Founder of the spin off SENSIA.